Relationships among Lightning, Precipitation, and Hydrometeor Characteristics over the North Pacific Ocean*

ANTTI T. PESSI AND STEVEN BUSINGER

School of Ocean and Earth Science and Technology, University of Hawaii at Manoa, Honolulu, Hawaii

(Manuscript received 29 June 2007, in final form 25 July 2008)

ABSTRACT

Lightning data from the Pacific Lightning Detection Network (PacNet) and Lightning Imaging Sensor (LIS) on the Tropical Rainfall Measuring Mission (TRMM) satellite were compared with TRMM precipitation radar products and latent heating and hydrometeor data. Three years of data over the central North Pacific Ocean were analyzed. The data were divided into winter (October–April) and summer (June–September) seasons. During the winter, the thunderstorms were typically embedded in cold fronts associated with eastward-propagating extratropical cyclones. Summer thunderstorms were triggered by cold upper-level lows associated with the tropical upper-tropospheric trough (TUTT). Concurrent lightning and satellite data associated with the storms were averaged over 0.5° × 0.5° grid cells and a detection efficiency correction model was applied to quantify the lightning rates. The results of the data analysis show a consistent logarithmic increase in convective rainfall rate with increasing lightning rates. Moreover, other storm characteristics such as radar reflectivity, storm height, ice water path, and latent heat show a similar logarithmic increase. Specifically, the reflectivity in the mixed-phase region increased significantly with lightning rate and the lapse rate of Z decreased; both of these features are well-known indicators of the robustness of the cloud electrification process. In addition, the height of the echo tops showed a strong logarithmic correlation with lightning rate. These results have application over data-sparse ocean regions by allowing lightning-rate data to be used as a proxy for related storm properties, which can be assimilated into NWP models.

1. Introduction

Accurate knowledge of the distribution and evolution of moisture and latent heating fields associated with deep convection is essential for accurate numerical forecasts of cyclogenesis (e.g., Anthes et al. 1983; Brennan and Lackmann 2005). The paucity of in situ observations over the North Pacific Ocean can lead to significant errors in the initial moisture fields' input into operational numerical models. These observational errors in turn often lead to large forecast errors in simulated storm geopotential height, wind, and rainfall (e.g., McMurdie and Mass 2004).

Radiosonde and weather radar sites are limited to a few Pacific islands that are generally located thousands of kilometers apart. Moreover, effective radar scans extend only ~200 km from the radar. Some low-orbit satellites offer information concerning convective activity, but they typically only have twice-per-day coverage. Geostationary satellites offer continuous monitoring of clouds and water vapor on visible and infrared channels, but cirrus clouds often obscure convective activity.

The next-generation series of the Geostationary Operational Environmental Satellite (GOES-R) are scheduled to be equipped with Geostationary Lightning Mappers (GLM) (Christian 2006) that will monitor lightning activity continuously over a wide field of view. Until these instruments are in orbit, tested and calibrated, ground-based lightning detection remains the only method to provide a continuous lightning data stream. The launch of the first GOES-R series satellite is scheduled for 2015.

Long-range lightning detection networks utilize the waveguide between the earth's surface and the ionosphere. The waveguide allows very low frequency (VLF) electromagnetic waves generated by lightning strike

* School of Ocean and Earth Science and Technology Contribution Number 7629.

Corresponding author address: Steven Businger, Department of Meteorology, University of Hawaii at Manoa, 2525 Correa Rd., Honolulu, HI 96822.
E-mail: businger@hawaii.edu

DOI: 10.1175/2008JAMC1817.1

channels to travel thousands of kilometers. The Pacific Lightning Detection Network/Long-Range Lightning Detection Network (PacNet/LLDN) is a network of widely spaced lightning detectors installed on the islands of the North Pacific (Fig. 1) to monitor thunderstorm activity over the North Pacific Ocean (Pessi et al. 2009). PacNet/LLDN (hereinafter just PacNet) is one of the few observing systems, outside of geostationary satellites, that provides continuous real-time data throughout a synoptic-scale coverage area over the open ocean. In Hawaii and the surrounding Pacific region, PacNet helps to fulfill a requirement for long-distance, real-time storm tracking.

A promising and important application of PacNet is to derive estimates of the rainfall rate and latent heating and hydrometeor profiles from lightning data over the Pacific Ocean that can be assimilated into numerical weather prediction (NWP) models. In areas of an NWP model domain for which the moisture content is underestimated, lightning data can contribute to forecast accuracy by adjusting the moisture fields and vertical profiles of latent heat release into the initial conditions and early forecast hours of the model in areas where lightning is observed (Alexander et al. 1999; Chang et al. 2001).

Numerous papers have documented the characteristics of oceanic storms and investigated the impact of various environmental conditions on storm development and electrification. Observational studies have documented convective storms over the oceans that contain little or no lightning, but have rainfall rates similar to active thunderstorms over land (e.g., Wang 1963; Zipser 1970, 1994; Takahashi 1978, 1990; Cram and Tatum 1979). Recently, satellite-based lightning and rainfall measurements have confirmed these observations (e.g., Nesbitt et al. 2000; Toracinta et al. 2002; Cecil et al. 2005; Futyan and DelGenio 2007a). This discrepancy can be explained in part by the efficiency of the warm rain process in the maritime environment (Pruppacher and Klett 1978). However, oceanic cumulonimbus clouds that reach the cold tropical tropopause can still show little or no lightning. Zipser and Lutz (1994) suggested that the updraft speed of the cloud must exceed a threshold value of 6–7 m s^{-1} to maintain a robust electrification process in the mixed-phase region. Observational studies have confirmed the relative weakness of the oceanic updrafts (LeMone and Zipser 1980; Zipser and LeMone 1980; Jorgensen and LeMone 1989; Lucas et al. 1994; Petersen et al. 1999). Rutledge et al. (1992) investigated the lightning rates and convective available potential energy (CAPE) during the monsoon season near Darwin, Australia, located on the northern coast. They showed that during low-CAPE periods (~500 J kg^{-1}), lightning was absent or the rates were very low. Lightning rates increased during periods of large CAPE (>1500 J kg^{-1}). However, CAPE values over the tropical oceans are not insignificant. Zipser and LeMone (1980) documented an average value of 1500 J kg^{-1} during the Global Atmospheric Research Program (GARP) Atlantic Tropical Experiment (GATE), where observed maximum vertical velocities in the top 10% of the storms were only ~5 m s^{-1}.

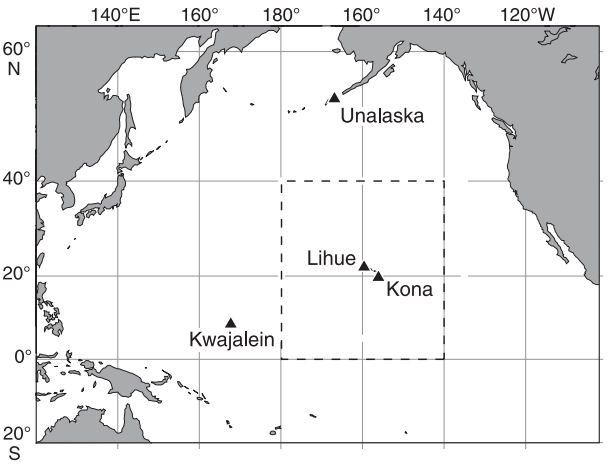

FIG. 1. Four sensors have been installed at Unalaska, Lihue, Kona, and Kwajalein. The LLDN sensors installed in North America contribute specifically over the eastern Pacific. Dotted rectangle shows the area of analysis in this study (adapted from Pessi et al. 2009).

Although CAPE may be substantial over the oceans, its vertical distribution can be significantly different between land and ocean. CAPE is often evenly distributed over a deep layer over the oceans, whereas it is concentrated within a shallow layer over land (e.g., Ebert and Holland 1992). McCaul and Weisman (2001) found in their numerical simulation that the stratification of the buoyancy had a great effect on the vertical velocity. When CAPE was concentrated in the low levels, the parcel vertical velocity was greatly enhanced. Thus, CAPE is an overly simplified measure of convective potential (Blanchard 1998).

Although the lightning climatology shows a reduced number of flashes over the ocean when compared with rates over adjacent continents, The Lightning Imaging Sensor (LIS) and Optical Transient Detector have observed a winter maximum over the North Pacific (e.g., Christian et al. 2003). PacNet data have also documented significant electrical activity over the North Pacific in a number of passing midlatitude cyclones (Pessi et al. 2009). Williams et al. (2000) and Boccippio et al. (2000) used Tropical Rainfall Measuring Mission (TRMM) LIS data to demonstrate that the majority of

the differences between land and ocean lightning rates can be accounted for by differences in storm density and frequency of occurrence, rather than differences in storm instantaneous lightning rates. This would suggest that the conditions for cloud electrification are less frequently met over the oceans than over the land, but once the conditions are met, the electrification mechanism is similar in maritime and continental storms, which has positive implications for data assimilation and NWP. Petersen et al. (2005) presented a similar argument that the environment can influence the degree to which the physical requirements for charge separation are met, but once the requirements are met, the basic physical process of charge separation is the same regardless of the regime (land, ocean, or coast). Therefore, they hypothesized that the relationship between ice mass and lightning density should be nearly regime invariant, which was verified in the consistent correlation found globally between precipitation ice water path (IWP) and lightning flash density. Sherwood et al. (2006) show that the global climatological maximum in lightning rates is linked to the small effective diameter of ice crystals near cumulonimbus cloud tops. This relationship was consistent both in continental and maritime environments.

The relationship between lightning and convective rainfall has been shown to vary up to three orders of magnitude, depending on airmass characteristics and cloud microphysics (e.g., Petersen and Rutledge 1998). However, several studies suggest that over a particular climatic regime and a limited geographic region, lightning is well correlated to convective rainfall (Chèze and Sauvageot 1997; Petersen and Rutledge 1998; Tapia et al. 1998; Soriano et al. 2001). Del Genio and Kovari (2002) used TRMM's Microwave Imager (TMI) and LIS data and categorized data into oceanic lightning and nonlightning, and land lightning and nonlightning storms. They found that the surface rainfall was much greater in the oceanic lightning than nonlightning storms, and the precipitation IWP varied ~30% between these two categories.

In this study, we used PacNet lightning rates corrected for network detection efficiency (DE) and TRMM satellite data matched in space and time to study the relationships between oceanic lightning, precipitation, and hydrometeor characteristics.

2. Data and methods

a. PacNet and data

The domain of this study is centered over Hawaii (0°–40°N, 140°W–180°) (Fig. 1). Currently PacNet consists of four long-range VLF sensors installed on the island of Kauai and the Big Island (Hawaii), Unalaska (Alaska), and Kwajalein (Marshall Islands). Further expansion of the network to the western Pacific is in progress. Data from LLDN are included in the data processing. LLDN sensors are conventional broadband LF/VLF sensors installed in the United States and Canada [North American Lightning Detection Network (NALDN)], but make a valuable contribution to the network, especially over the eastern Pacific. A detailed description of PacNet is given in Pessi et al. (2009).

The fourth PacNet sensor was installed in Kona, Hawaii, in February 2004. Therefore, 3 yr of data (February 2004–February 2007) were used in this study. All the TRMM orbits, when LIS detected any lightning over the central Pacific, were included in the analysis (over 2000 overpasses).

The detection efficiency of the PacNet varies both spatially and temporally, because of the geometry of the sensor sites and the diurnal variation of the reflectivity of the ionosphere. A DE model (Pessi et al. 2009) was applied to the lightning data stream to take this variability into account and adjust the lightning rates (Fig. 2). The finite location accuracy of PacNet (Pessi et al. 2009) was taken into account by smoothing the lightning density field so that the lightning density in each grid cell accounted for 70%, and the eight grid cells surrounding the cell accounted for the remaining 30% of the total lightning density in each cell.

The PacNet lightning data used in this study were quality controlled as follows: (i) Only the days when at least three PacNet sensors (Lihue, Kona, Unalaska + LLDN) were up were included in the analysis. (ii) Duplicated flash locations were removed from the database. A single lightning strike is often detected as two or more PacNet events. Multiple sky-wave locations are possible, because more than one ''collection'' of sensors can experience a group-consistent propagation path delay. In contrast, there is only one (or zero) groundwave location. Error statistics were used to select between multiple PacNet locations. The error-ellipse semimajor axis (SMA) and angle and time deviations (χ) are associated with each flash and represent the quality of the location. If there were multiple locations within 1 μs, the flash with the smallest value of $\mathrm{SMA}/\sqrt{\chi}, (\chi \geq 1)$ was chosen to represent the flash location. (iii) Only the area, where the projected location accuracy of PacNet was better than ~15 km, was included in the analysis (Pessi et al. 2009). Data were also excluded in the areas where the modeled DE was <3% (in the immediate vicinity of the Hawaiian sensors where DE approaches zero because of the network geometry, and in remote corners of the domain; Fig. 2). PacNet data quality control results in a small reduction

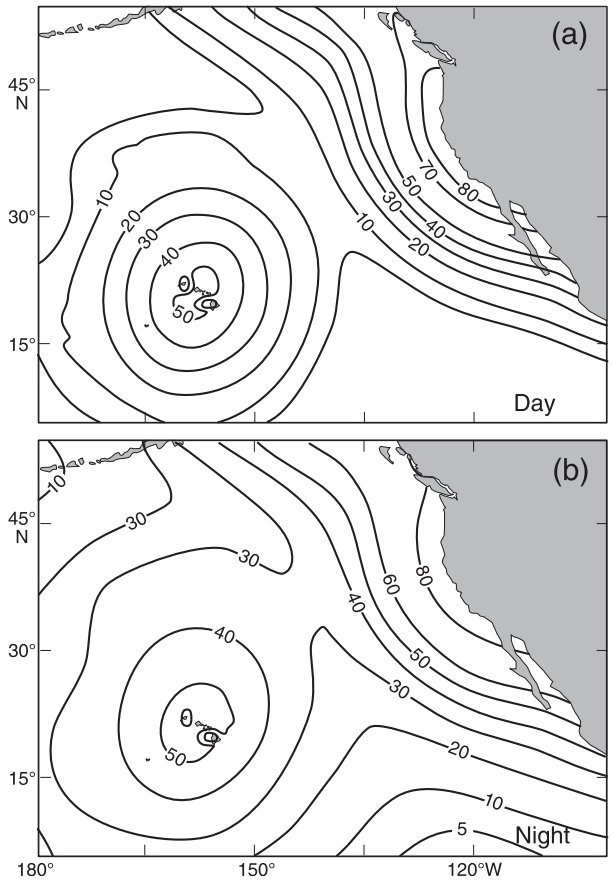

FIG. 2. Detection efficiency (%) of PacNet during (a) day and (b) night (adapted from Pessi et al. 2009).

in the dataset over the 3-yr period. Data from storms missing from the PacNet dataset may be present in the LIS database, resulting in a slightly different set of storms included in the two databases. Given the climatological nature of the study, this difference in the databases is justifiable, as will be discussed in section 3.

b. TRMM data

Since the orbital inclination of the TRMM satellite is 35°, TRMM data are available within the latitude band from approximately 38°N to 38°S, depending on the swath width of the instrument (e.g., Kummerow et al. 1998). Precipitation radar (PR) 2A25 (version 6) products are used in this study, including estimated surface rainfall, precipitation water path, and vertical profiles of radar reflectivity (Iguchi et al. 2000). PR measures the reflectivity at 80 range bins from surface to 20-km altitude with 250-m vertical resolution. The horizontal sampling resolution is 4.3 km.

The 2A25 PR pixels identified as ''convective'' (as in 2A23 Rain Type Flag) were used in this study. The only exception to this is the result presented in section 3d, where estimated surface rainfall rates from pixels identified as ''stratiform'' are shown and compared to convective rain rates. The rainfall rates used in this study are the 2A25 estimated surface rain rates. These are calculated by assuming a constant slope of dBZ_e from the bottom of the clutter-free rain echo.

In addition, 2A12 version 6 products are used, including vertical profiles of latent heating and precipitable ice in 14 layers with 5-km horizontal resolution. Below 4 km, the vertical resolution is 0.5 km and the resolution decreases upward to 4 km in the highest layer, 14–18 km above the surface.

The TMI measures the intensity of radiation at five separate frequencies: 10.7, 19.4, 21.3, 37.0, and 85.5 GHz. The 2A12 algorithm searches a large database of cloud resolving model (CRM) simulations to find cloud profiles that are radiatively consistent with TMI radiance measurements. The retrieved profile is a composite of those consistent profiles (Kummerow et al. 2001). Some 2A12 products, such as cloud ice data, should be interpreted cautiously, since small ice particles do not have microwave signatures, and the vertical cloud ice profiles are solely products of the cloud resolving models. In version 6 of 2A12, a significant improvement of the Bayesian estimation method was implemented. The revised algorithm is supported by an expanded and physically more consistent database of cloud model simulations. The CRM simulation database now includes both Goddard Cumulus Ensemble (GCE) and the fifth-generation Pennsylvania State University–National Center for Atmospheric Research Mesoscale Model (MM5) simulations of a tropical cyclone, tropical squall lines over the Pacific and Atlantic, tropical convection over the Pacific, and two extratropical cyclones in the North Atlantic. One of the simulated Atlantic extratropical cyclones occurred in the summer and one in the winter. Both warm and cold frontal regions of the cyclones were simulated. In addition, several other modifications were included to allow better estimates of the storm properties, with a specific goal to obtain improved estimates of the latent heating profiles over the ocean surfaces. The algorithm is described in detail in Olson et al. (2006) and Yang et al. (2006). This was the first attempt to include latent heating estimations within the framework of 2A12. An improved algorithm, which utilizes the same Bayesian framework as 2A12, but with a training database derived from PR observations, is described in Grecu and Olson (2006).

TRMM also carries LIS, which contains an optical staring imager that detects brightness changes in the clouds as they are illuminated by lightning discharges (Christian et al. 1992). LIS can detect cloud-to-ground (CG), cloud-to-cloud, and intracloud (IC) lightning. LIS

views a 600 km × 600 km area with a spatial resolution of 4 km at nadir and 7 km at limb. One downside of LIS is that it observes every point within its field of view for only ~90 s, which makes weak oceanic storms with lightning rates less than ~1 flash per minute undetectable by LIS (Boccippio et al. 2000). Lightning rates are corrected for diurnally varying LIS detection efficiency using the DE values of 73% (93%) for day (night) estimated by Boccippio et al. (2002).

c. Methods

TRMM-derived products were averaged over 0.5° latitude × 0.5° longitude grid cells. Lightning strikes from PacNet that occurred within ±15 min of the satellite overpass time over the same grid cells were counted. Both LIS and PacNet lightning counts were normalized as flashes per 10^4 kilometers squared per hour. The size of a 0.5° grid cell is a function of latitude and was taken into account in the normalization. LIS observation time of 90 s was used for normalization.

The observations show a logarithmic decrease in observation count with increasing lightning rate (Fig. 3). The logarithmic shape of the cumulative probability distribution function (PDF) suggests dividing the lightning data into bins using a logarithmic division [e.g., values between 2^n and 2^{n+1} flashes × $(10^4\ \text{km}^2\ \text{h})^{-1}$ formed a bin (n = integer)]. Using this method, the bins plotted on a logarithmic axis are nearly equidistant. Because of the low number of samples in the highest bin, the two highest bins were combined for both winter and summer data.

Lightning flashes detected by PacNet are mostly cloud to ground, whereas LIS detects both cloud-to-ground and intracloud flashes. LIS flash rates are not corrected for the IC:CG ratio in this study, as the ratio varies with storm type and stage, environmental conditions, and domain (Pierce 1970; Prentice and Mackerras 1977; Mackerras et al. 1998; Boccippio et al. 2001; Pessi et al. 2009). The impact of this on the results is discussed in section 3a.

3. Results

Three years of active lightning days were analyzed over the central North Pacific Ocean during 2004–07. Most of the summer storms were associated with upper-tropospheric disturbances during July–August (e.g., Fig. 4), when a tropical upper tropospheric trough (TUTT) is most pronounced over the central Pacific (Sadler 1975; Kelley and Mock 1982). Typically during these storms, an upper-level low pressure center (TUTT cell) with a well-defined circulation and cold temperatures aloft was evident in the upper-level charts (Fig. 4b). Surface

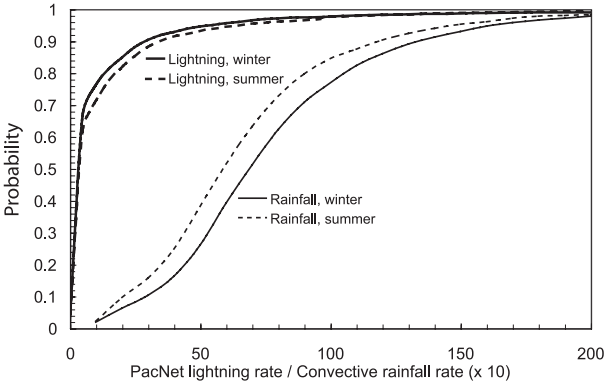

FIG. 3. Cumulative PDF for PacNet lightning rate [flashes × $(10^4\ \text{km}^2\ \text{h})^{-1}$] and PR convective rainfall rate (mm h^{-1} × 10). The x axis is suppressed with ~99% of the highest rates shown.

maps showed little sign of a surface trough during the weakest storms, but a surface trough was associated with the stronger storms (Fig. 4c).

During the winter, most of the lightning activity was associated with extratropical storms and kona lows (Morrison and Businger 2001; Otkin and Martin 2004; Caruso and Businger 2006), and in particular with convection along cold fronts or well-defined troughs at the surface and aloft (Fig. 5). Although most of the storm centers stay north of Hawaii, the cold fronts and associated cold upper-level troughs often reach the islands and cause the majority of the annual lightning and severe weather events locally in Hawaii (e.g., Businger et al. 1998).

The 2A12 version 6 database, discussed in section 2b, includes both extratropical winter frontal systems and summer convective systems. Therefore, it is expected that 2A12 adequately represents both the winter and summer storms. However, since 2A12 is still under development (specifically the latent heating algorithm), the results from 2A12 should be interpreted as preliminary.

a. Maximum radar reflectivity and altitude of the echo top

Maximum radar reflectivity, corrected for attenuation, is a 2A25 product given for each radar beam, with the maximum often observed at the lowest levels. Maximum reflectivity ($Z_{\max}$) increases with lightning rate from 33 to 41 dBZ in the winter and from 32 to 40 dBZ in summer (Fig. 6a). Increasing radar reflectivity with increasing lightning rate is expected, because the cloud electrification increases with ice mass (e.g., Takahashi 1984; Petersen et al. 2005). The reflectivity is slightly higher in the winter than in the summer. This observation will be discussed later in this section together with

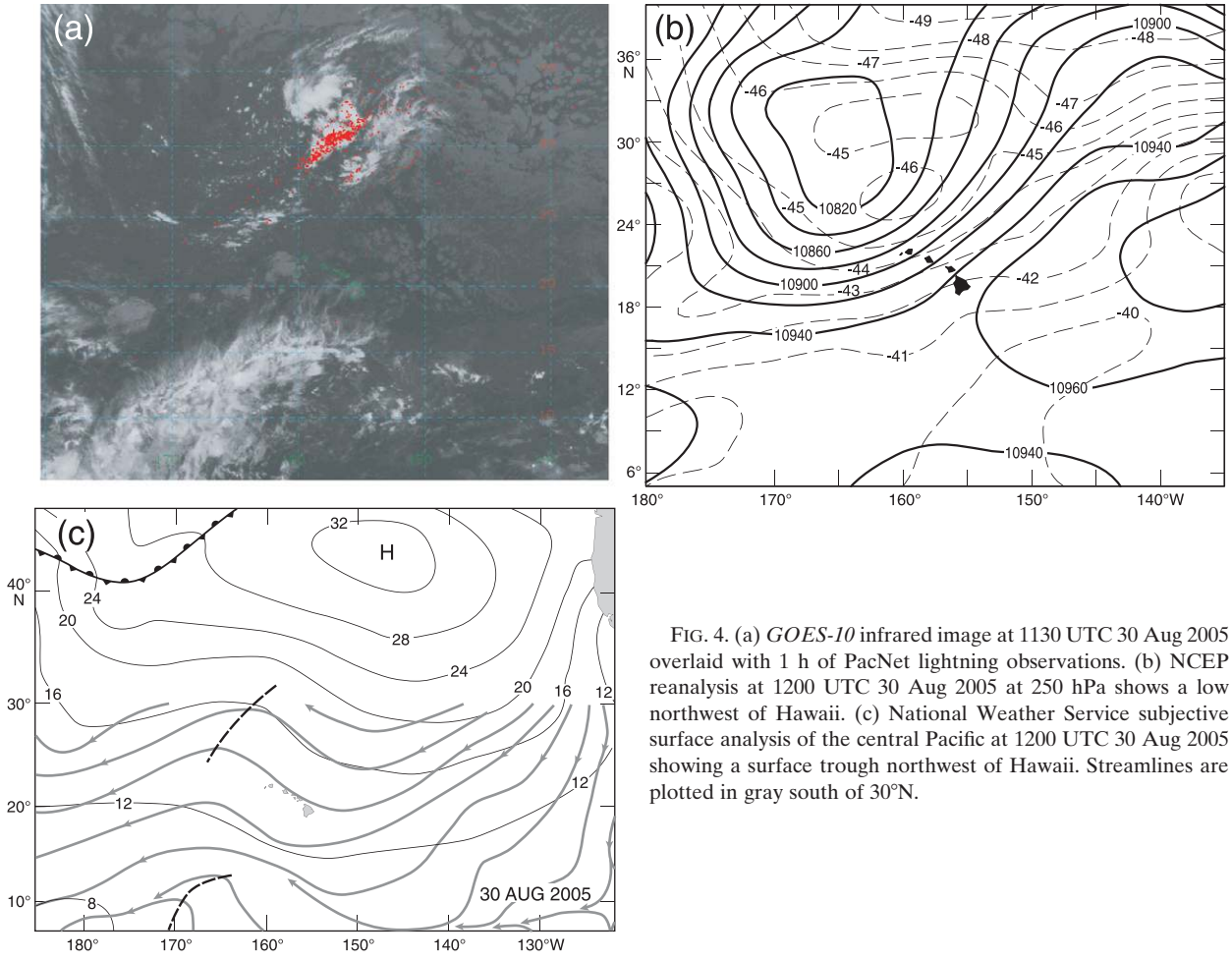

FIG. 4. (a) *GOES-10* infrared image at 1130 UTC 30 Aug 2005 overlaid with 1 h of PacNet lightning observations. (b) NCEP reanalysis at 1200 UTC 30 Aug 2005 at 250 hPa shows a low northwest of Hawaii. (c) National Weather Service subjective surface analysis of the central Pacific at 1200 UTC 30 Aug 2005 showing a surface trough northwest of Hawaii. Streamlines are plotted in gray south of 30°N.

precipitation and ice mass. The variance decreases with increasing lightning rate, which can be attributed to the logarithmic nature of the radar reflectivity, where a certain variability of hydrometeor mass shows as large (small) variance in the reflectivity at the low (high) end of the scale. This relationship will be confirmed in section 3d with the discussion of rainfall rates.

The echo-top altitude increases with lightning rate from approximately 6.7 to 12.8 km in the winter and from 7.0 to 13.5 km during the summer (Fig. 6b). The increasing echo-top altitude with lightning rate is likely connected to the vigor of the updrafts, with more precipitation-size particles transported higher in the troposphere with stronger updrafts. Futyan and DelGenio (2007b) investigated the height of the convective storms over the African–Atlantic region and also found a strong correlation between the PR echo-top altitude and LIS flash rates. Other studies have also found a correlation between the cloud-top height and lightning rate (Williams 1985; Price and Rind 1993). Furthermore, Price and Rind (1993) showed that the IC:CG ratio increases as the cloud thickness increases. It should be noted that the echo top detected by TRMM's PR is not equivalent to cloud-top height, because PR does not detect the smallest cloud droplets at its 13.8-GHz frequency. The sensitivity threshold for PR is ~17 dBZ.

In Fig. 6b, variance decreases with increasing lightning rate, similarly to Fig. 6a. However, as opposed to Fig. 6a, this feature is real and not an artifact of the scale. This occurs presumably because the strongest storms grow upward until they reach the tropopause, which reduces the variance at the high end of the altitude scale. The echo tops are found at slightly higher altitude during the summer than in the winter, because both the freezing level and the tropopause are at a higher level during the summer. Coefficients of determination (R^2) in both Figs. 6a and 6b are between 0.95 and 0.98.

Lightning rates are generally higher in LIS than in the PacNet dataset (Fig. 6). This is partly because of LIS's

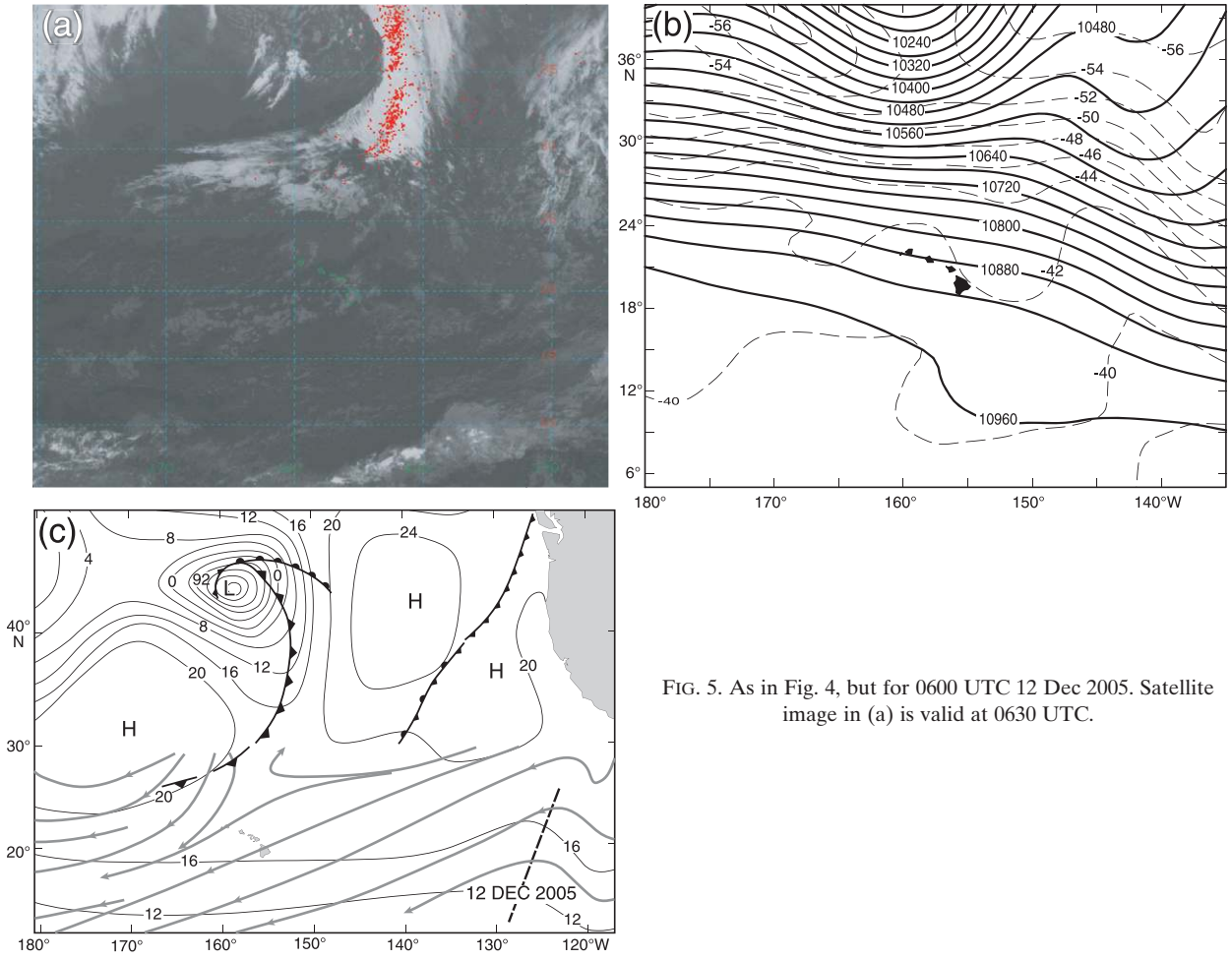

FIG. 5. As in Fig. 4, but for 0600 UTC 12 Dec 2005. Satellite image in (a) is valid at 0630 UTC.

intracloud observations and partly because of LIS's view time and limited ability to observe weak oceanic storms. The impact of applying an IC:CG correction to LIS data would be to shift the LIS data points to the left in Fig. 6 (and other figures with lightning rate as an abscissa) according to the IC:CG ratio. However, if the results derived from LIS observations in this study are applied in the future LIS observations, no IC:CG correction is needed, as the same bias exists in both datasets. A similar argument applies for PacNet data.

The detection threshold for LIS is ~1 flash per minute (Boccippio et al. 2000). If LIS detects one flash during an overpass over a 0.5° grid cell, the area-normalized minimum flash rate is ~150 flashes $\times$ $(10^4\ \text{km}^2\ \text{h})^{-1}$ (at 20°N, using nighttime DE of 0.93, and 90-s view time). This value is at the high end of PacNet observations (Fig. 6). In addition, some very active thunderstorms occurred near the date line, which were included in the LIS analysis but were filtered from PacNet analysis because of PacNet's limited location accuracy over that area (section 2a). The highest non–quality controlled PacNet lightning rates over this area were ~3700 and 940 flashes $\times$ $(10^4\ \text{km}^2\ \text{h})^{-1}$ for winter and summer, respectively. These values are closer to the middle and high end of the LIS flash rates.

In comparing to previous studies, care must be taken with the units. The average lightning rates in the highest bins were 12 138 and 7729 flashes [$\times$ $(10^4\ \text{km}^2\ \text{h})^{-1}$] for winter and summer in this study, respectively. Two previous studies used a similar 0.5° grid to investigate oceanic lightning and have found lightning rates of similar magnitude to those reported here. Petersen et al. (2005) divided their warm-season lightning observations into maritime, coastal, and continental categories. The highest maritime lightning bin was ~5 flashes per kilometers squared per day, which converts to ~2083 flashes $\times$ $(10^4\ \text{km}^2\ \text{h})^{-1}$. Futyan and DelGenio (2007b) investigated storm heights over convective cloud clusters in the Atlantic–African region. The highest lightning rates over the oceanic systems were ~1 flash per 300 kilometer squared per minute, which equals 2000 flashes $\times$ $(10^4\ \text{km}^2\ \text{h})^{-1}$. The lower lightning rates found in Futyan

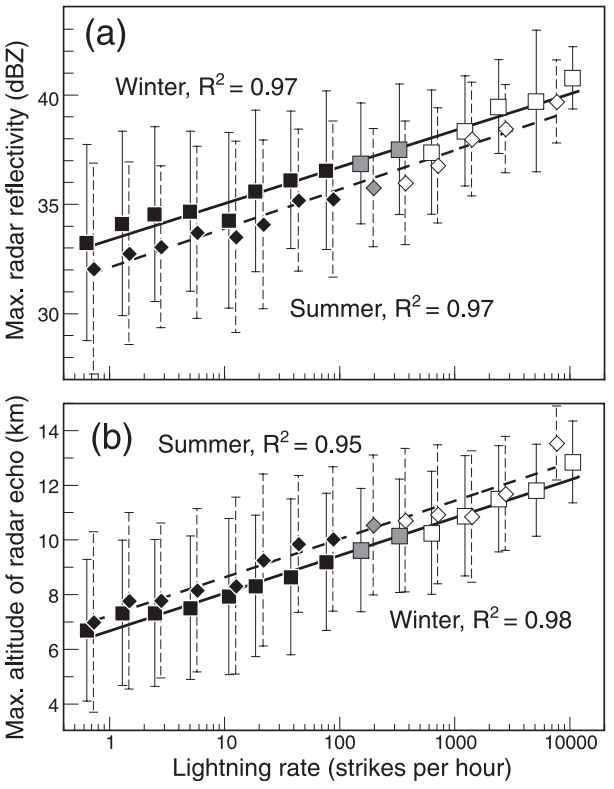

FIG. 6. (a) Maximum PR reflectivity and (b) maximum height of radar echo. Squares and solid lines are for winter data and diamonds and dashed lines for summer data. Filled symbols are PacNet data, open symbols are LIS data, and gray symbols are combined PacNet and LIS data. Abscissa shows the number of lightning flashes per hour normalized over 10^4 kilometers squared. The error bars are $\pm 1\sigma$.

and DelGenio than in this study may be due to a smaller sample size and lack of high lightning rate storms. The highest individual pixel value in Petersen et al. corresponded to ~25 000 flashes $\times$ $(10^4$ km^2 h$)^{-1}$, whereas the highest lightning rates in this study were 25 274 and 23 694 flashes $\times$ $(10^4$ km^2 h$)^{-1}$ for summer and winter, respectively.

b. *Vertical profiles of radar reflectivity, latent heat, and ice*

Vertical profiles of radar reflectivity have been found to be an important indicator of cloud electrification and lightning activity (e.g., Zipser and Lutz 1994; Petersen et al. 1996; Toracinta et al. 1996, 2002; Nesbitt et al. 2000). Several studies have shown that the main thunderstorm charging mechanism is the ice–ice collision process, where the riming graupel particles collide with smaller ice particles in the presence of supercooled water (e.g., Saunders 1993). This process occurs in the mixed-phase region, from 0° to −20°C, and is the most efficient from −10° to −20°C. Radar reflectivity can be used to estimate the amount of mass present in the mixed-phase region, which is an important indicator of the robustness of the charging process. The suggested vertical velocity threshold of 6–7 m s^{-1} (Zipser and Lutz 1994) can support raindrops in the 1.2–1.5-mm range at −10°C (e.g., Foote and Du Toit 1969) and therefore provide an adequate hydrometeor source for electrification.

Radar reflectivity shown in Fig. 7 is a separate 2A25 product from maximum attenuation-corrected radar reflectivity in Fig. 6a. Therefore, the lowest-level reflectivity (Z) in Fig. 7 should not be confused with $Z_{\max}$ values shown in Fig. 6a. However, the maximum reflectivity tends to occur at the lowest levels, making the difference relatively small. Figure 7 shows that radar reflectivity increases with lightning rate throughout the troposphere. Table 1 summarizes the values found for several altitude (or temperature) and reflectivity thresholds. The average freezing levels given in 2A25 data for winter and summer storms are 3.7 and 4.0 km, respectively. Applying an average −6.5°C km^{-1} temperature lapse rate, the levels of −10° and −20°C are ~1.5 and ~3 km above the freezing level, respectively.

Earlier studies have shown that the decrease in radar reflectivity with height in the mixed-phase region is much greater for oceanic than for continental thunderstorms. Estimates of the lapse rate for the oceanic regime vary between 6.0 and 6.5 dBZ km^{-1} (Jorgensen and LeMone 1989; Szoke et al. 1986; Zipser and Lutz 1994). In sharp contrast, continental storms show much lower lapse rates, between 1.3 and 2.0 dBZ km^{-1} (Donaldson 1961; Zipser and Lutz 1994). In this study, the lapse rate varied between 5.3 and 3.0 dBZ km^{-1} for low lightning rate winter storms and for high lightning rate storms, respectively.

The 0-dBZ thresholds are found at slightly higher altitude in the summer than in the winter, probably because of the higher tropopause height. In the highest category, there is a noticeable bump in the summer data between approximately 6- and 10-km altitude. A similar feature is observed in the latent heating profile, which shows a secondary peak between 7- and 11-km height (Fig. 8b). This corresponds approximately to temperatures between −20° and −45°C in the troposphere. The peak may be partly attributed to the latent heat of fusion by homogeneous freezing of supercooled water droplets. The temperature threshold for homogeneous freezing is ~−36°C (e.g., DeMott and Rogers 1990; Phillips et al. 2007). A typical −36°C level in the area (based on soundings from Lihue, Hawaii) varies between 9200 and 10 200 m in June–September. Below this level, the secondary peak in latent heating may be associated with heterogeneous ice nucleation and riming of existing ice particles.

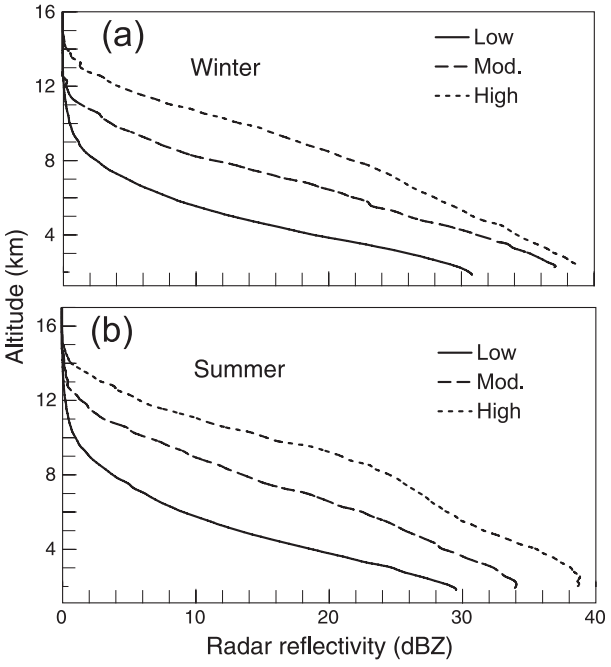

FIG. 7. Vertical profiles of PR reflectivity in (a) winter and (b) summer for three different lightning rate categories (low, moderate, and high lightning rate). Low lightning rate category is the lowest bin from PacNet data, moderate category is the highest PacNet data bin, and high category is the highest LIS bin, as described in section 2c. The average lightning rates in the low, moderate, and high categories are ~1, 383, and 12 138 flashes [$\times$ (10^4 km^2 h)$^{-1}$] in the winter. The corresponding values for the summer are ~1, 214, and 7729 flashes. Lowest levels are not shown since the near-surface range bins were frequently filled with surface clutter or had missing data. Despite a sensitivity threshold for PR echoes of ~17 dBZ, values start from zero because of the compositing method.

Vertical latent heating profiles are 2A12 products that combine both convective and stratiform profiles. The low lightning rate curves show a double-peak shape (Fig. 8). This may be due to the shape of the stratiform profile, often characterized by evaporative cooling at 2–3-km altitude (as illustrated in Olson et al. 2006). This feature disappears in the high lightning rate storms, where the convective-shaped curve presumably dominates over stratiform, as shown in Fig. 8. Both winter and summer data show strong evaporative cooling near the surface.

Maximum latent heating rates were obtained by taking the highest latent heating values occurring at any TMI level (Fig. 8c). The level of maximum latent heating is usually at 2–3-km altitude and does not change significantly with lightning rate, although a little lift is observed during the summer (Figs. 8a,b). The maximum latent heating increases with lightning rate, consistent with Figs. 8a and 8b. Although the R^2 values are high (0.94), variance is very large. Again, this may be because of the uncertainties in the latent heating algorithm, or because of complex storm dynamics.

Although the maximum latent heating at the 2–3-km level consistently increases with increasing lightning rate, winter data show an odd feature. The latent heating rate in the highest category decreases rapidly with altitude above 2 km and reaches the same value at ~4 km as the lowest category (Fig. 8a). Sensitivity tests performed using different samples of high lightning rate data did not change the result; the highest lightning rate storms have less latent heating above ~3 km than moderate lightning rate storms. A similar feature is observed in the precipitable ice profiles, where the profile for the highest lightning category in winter has a greater peak ice content than the moderate category (at ~4 km), but has a lower content above 5 km (Fig. 9a).

The most lightning-active winter storms occurred in the cold front or in the cold air mass behind the front, where the freezing levels are low. This in turn may result in a system with large quantities of ice at low levels decreasing rapidly upward. Subsequently, the negative charge center develops at relative low altitude, resulting in a large number of negative CG flashes.

Although the highest lightning category in the winter shows little ice above ~5 km, the reflectivity in Fig. 7a does not show any unusual decrease in this altitude range. This suggests that there are other hydrometeors than ice accounting for the reflectivity. Other possible reasons for this may be an insufficient 2A12 database or uncertainties in the latent heating and ice algorithms. This will be discussed in the next subsection together with precipitation and ice water paths.

However, the altitude of the peak ice content during the winter seems to decrease with increasing lightning categories (from ~5 to ~3.5 km), although this difference

TABLE 1. Summary of heights and reflectivities at various dBZ and altitude thresholds.

Winter (summer)	20 dBZ	30 dBZ	0°C [3.7 (4.0) km]	−10°C [5.2 (5.5) km]	−20°C [6.7 (7.0) km]	Avg lapse rate of Z (0°C...−20°C)
Low lightning rate	3.8 (3.7) km	2.2 (N/A) km	21 (19) dBZ	11 (11) dBZ	5 (6) dBZ	5.3 (4.3) dBZ km^{-1}
Moderate lightning rate	6.4 (6.5) km	4.2 (3.6) km	31 (28) dBZ	25 (24) dBZ	18 (18) dBZ	4.3 (3.3) dBZ km^{-1}
High lightning rate	8.4 (9.2) km	5.3 (5.5) km	35 (36) dBZ	30 (30) dBZ	26 (27) dBZ	3.0 (3.0) dBZ km^{-1}

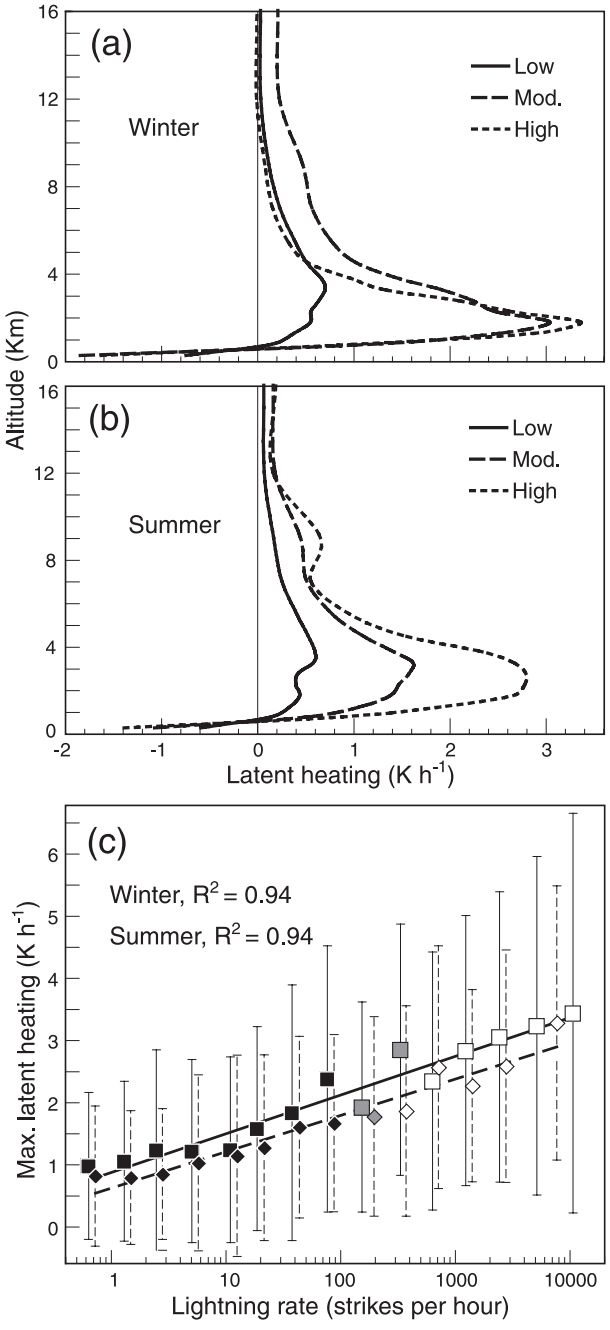

FIG. 8. Vertical profiles of latent heating in (a) winter and (b) summer for low, moderate, and high lightning rates. (c) Maximum latent heating rate vs lightning rate. Lines and symbols as in Figs. 6, 7.

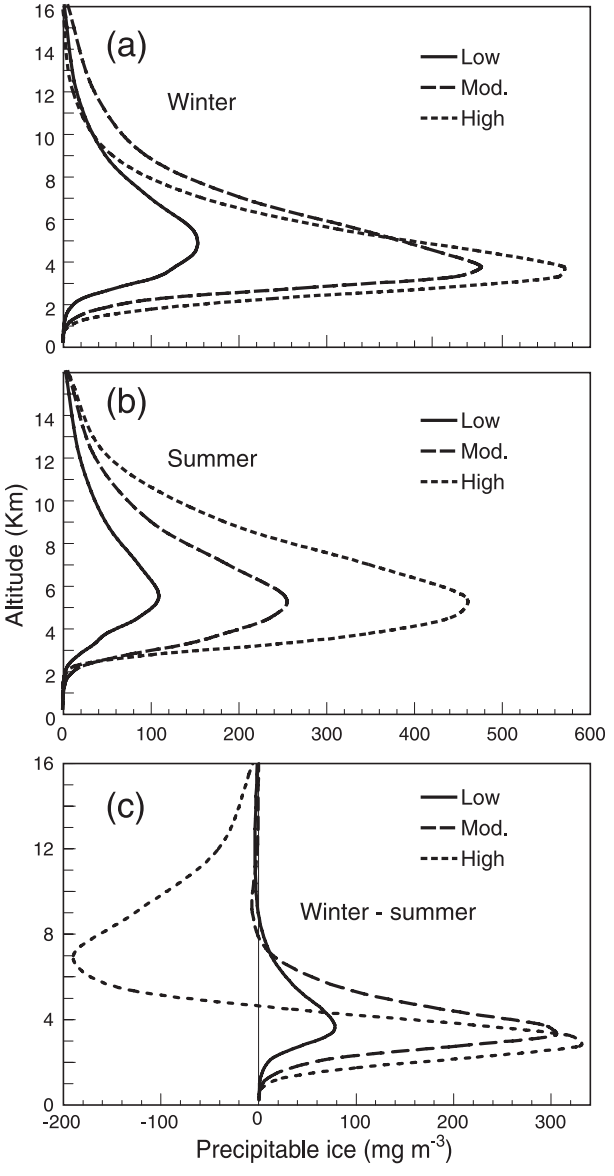

FIG. 9. As in Fig. 7, but for precipitable ice content, derived from TMI data, as a function of height and lightning rate. (c) Difference between winter and summer.

is ~1 TMI level (Fig. 9a). In the summer, the level of the peak ice content is nearly the same for each lightning category (Fig. 9b). Given the limited 2A12 winter database and uncertainties in the algorithm, these subtle differences in altitude should be interpreted with caution.

Despite some odd features in the profiles, the peak precipitable ice content generally increases with lightning rate both in winter and summer (Figs. 9a,b). The level of maximum precipitable ice shifts upward from winter to summer, whereas the peak content decreases. The peak precipitable ice content is observed just above the freezing level for both winter and summer (3.5–5.0 and 4.0–6.0 km, respectively). Some ice is also observed below the freezing level, which may be solid precipitation particles falling down from upper levels.

The difference in precipitable ice between winter and summer shows that there is more ice during the winter at low levels (3–4 km) (Fig. 9c). This can be explained by the lower freezing level during the winter. However,

in the highest lightning category, there is significantly more ice above ~5 km in the summer. Naturally, this is partly accounted for by the low ice content above 5 km in the winter data. The reason for this may be the stronger updrafts in the mesoscale convective system type summer systems that can lift large ice particles to high altitudes, as opposed to forced slantwise lift in winter frontal systems where the vertical velocity is modest and the storms are shallower.

Del Genio and Kovari (2002) investigated tropical oceanic lightning and nonlightning storms and constructed profiles of precipitable ice content. They found a maximum precipitable ice content of 320 mg m^{-3} in oceanic storms both with and without lightning. In this study, the maximum content varied between 100 and 600 mg m^{-3} (Fig. 7).

The highest lightning categories in the winter and summer showed different lightning rates. This partition was chosen because we wanted to compare the strongest systems during both seasons. However, additional tests were performed where the winter lightning rates were similar to those in the highest summer category. This did not change the results qualitatively: when winter and summer storms with similar lightning rates were compared, significantly more precipitable ice was found above 5 km in the summer storms.

c. Precipitation water path and ice water path

Precipitation water path (PWP) from PR data is the vertically integrated precipitation water content calculated from Z_e at each range bin, from rain top to the surface. Both liquid and solid phase regions are included in the calculation. PWP increases with lightning rate with very little difference between summer and winter (Fig. 10a).

Ice water path is calculated from 2A12 vertical precipitable ice profiles as observed by TMI; IWP increases with lightning rate with slightly higher values during the winter in the low and moderate lightning rates (Fig. 10b).

As discussed in the introduction, the existence of ice and supercooled water in the mixed-phase region is essential for cloud electrification. Increasing reflectivity (Figs. 6a, 7) and precipitable ice (Figs. 9a,b) are consistent with increasing precipitation mass with lightning rates (Fig. 10).

Although the R^2 values are a little higher in IWP than in PWP data, the variance is significantly lower in PWP data. This may be partly due to the robustness of the PR observations and 2A25 in comparison with TMI observations and 2A12 algorithm.

As discussed earlier, the strongest storms in the winter showed very little ice above 5 km, whereas the reflectivity did not show any unusual decrease. Figure 11a shows that the precipitation water increases steadily with lightning rate, whereas the ice water remains relatively steady between 2000 and 2200 g m^{-2} in the four highest lightning categories. In contrast, both PWP and IWP increase in the summer (Fig. 11b). This suggests that the strongest winter storms may have large quantities of supercooled liquid water at high altitudes.

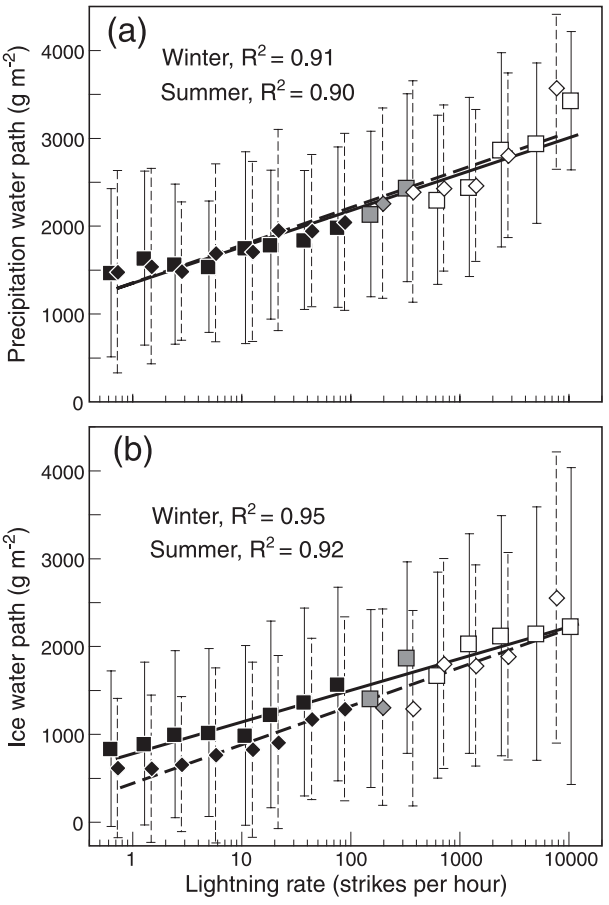

FIG. 10. (a) Precipitation water path derived from PR and (b) ice water path derived from TMI. Lines and symbols as in Fig. 6.

d. Lightning versus rainfall

The lightning rates from both PacNet and LIS were compared to estimated surface rain from 2A25 convective pixels, as described in section 2. Although a direct comparison of reflectivity (Fig. 6a) to rainfall rates (Fig. 12a) seems appealing, it should be noted that the Z–R relationship used by 2A25 may vary with each scan. Parameters a and b in the relationship $R = aZ^b$ used by 2A25 are both functions of the rain type, the heights of the 0°C isotherm, and storm top. Furthermore, the presence or absence of a bright band, the phase state, the temperature, and the difference in terminal velocity

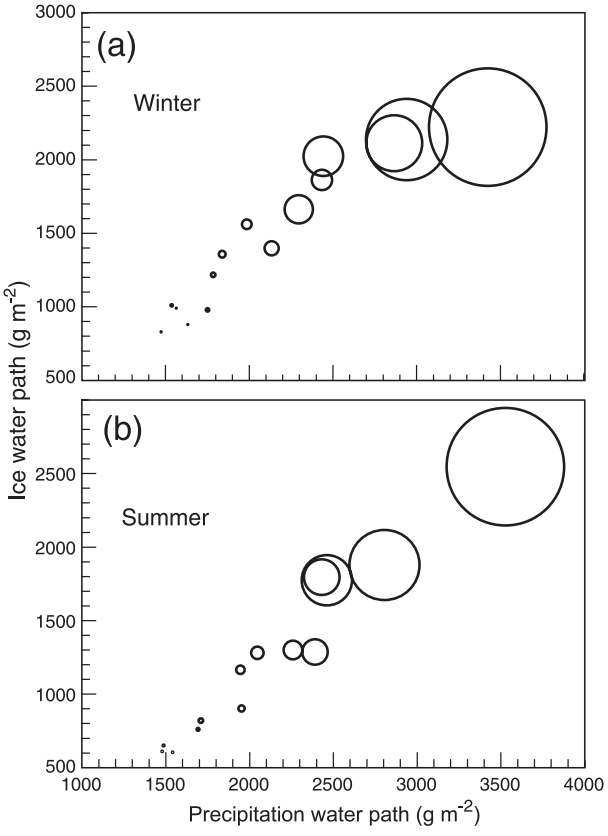

FIG. 11. Precipitation water path vs ice water path for (a) winter and (b) summer. The sizes of the open circles correspond to the lightning rates shown in Fig. 10.

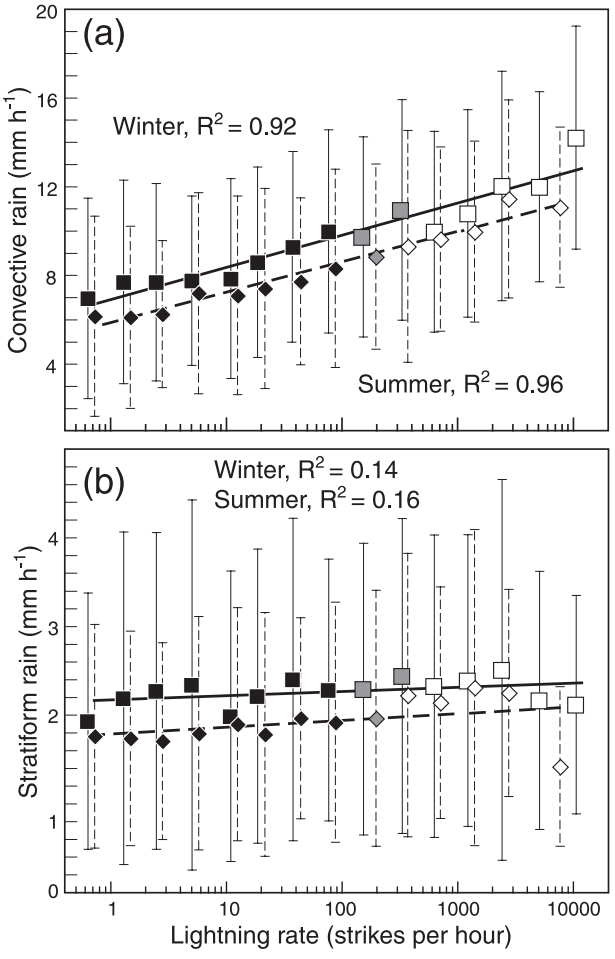

FIG. 12. (a) Convective rainfall vs lightning rate and (b) stratiform rainfall vs lightning rate. Symbols and lines as in Fig. 6.

from changes in the air density have an effect on parameters a and b (Iguchi et al. 2000).

Convective rainfall rate increases with lightning rate during both summer and winter (Fig. 12a). This result is not surprising, given that radar reflectivity increases with lightning rate. This in turn can be attributed to increased upward mass flux, which subsequently results in heavier convective precipitation. While the values of R^2 of the fitted curves were high (0.92 and 0.96 for winter and summer, respectively), the variance in each bin was relatively large. The standard deviation varied between 3.3 and 5.2 mm h^{-1}. The large variance is possibly a result of a variable portion of warm rain of the total convective rain in these maritime clouds. Winter rainfall rates were consistently 1–2 mm h^{-1} higher than in the summer.

In contrast, the stratiform rainfall was poorly correlated with lightning rate (Fig. 12b). Stratiform rain rates remained nearly constant at ~2 mm h^{-1} despite lightning rate or season. Although it could be argued that the amount of precipitable particles ejected from convective towers should increase with lightning rate and thus increase the stratiform rain rate, the results show that the anvil region seems to be relatively uniform despite the storm strength. This suggests that the majority of the particles carried up by the convective updrafts come down as convective rainfall.

4. Summary, conclusions, and discussion

The objective of this study is to investigate the correlation between lightning rates and various storm characteristics that are physically connected to lightning production via storm dynamics. These storm properties can then be estimated from lightning rates and assimilated into numerical models in data-sparse regions, such as the open oceans.

Long-range lightning data from the Pacific Lightning Detection Network and Lightning Imaging Sensor were compared with TRMM 2A25 precipitation radar and 2A12 hydrometeor products. The PacNet lightning

rates were quantified by applying a detection efficiency model correction to account for spatial and temporal differences in lightning detection efficiency over the domain.

Three years of lightning-active days during summer and winter were analyzed over the central North Pacific Ocean. The winter storms were mostly extratropical cyclones, with most of the electrical activity associated with cold fronts. The summer cases were mostly convective storms triggered by cold upper-tropospheric disturbances associated with the TUTT. Vertical profiles of radar reflectivity, latent heating, and precipitable ice were constructed.

a. Conclusions

The results of the data analysis show a consistent increase in radar reflectivity throughout the troposphere with lightning rate. Specifically, the reflectivity in the mixed-phase region increased significantly with lightning rate and the lapse rate of Z decreased; both are well-known indicators of the robustness of the cloud electrification process. In addition, the height of the echo tops showed a strong logarithmic correlation with lightning rate.

Convective rainfall rate showed a consistent logarithmic increase with increasing lightning rates. A similar slope in the lightning–convective rainfall relationship for both summer and winter cases indicates that over the central North Pacific, the average lightning–rainfall relationship is relatively independent of the season and storm type. Stratiform rain rate, however, was poorly correlated with lightning and remained nearly constant despite changes in the lightning rate.

Moreover, other storm characteristics such as precipitable ice, ice water path, and precipitation water path show a similar type of increase. The probability distribution function for PacNet lightning rate (Fig. 3) shows an exponential decrease in occurrence with increasing lightning rates.

The data analysis revealed an interesting feature in the strongest winter storms: the highest ice content together with latent heating appeared to be at low levels, decreasing rapidly upward. This may be attributed to the low altitude of the negative charge center in these cold–air mass thunderstorms, which results in a high number of negative cloud-to-ground flashes. Another possible explanation is the inadequate 2A12 winter database.

b. Discussion and future work

The probability distribution function for PacNet lightning rate (Fig. 3) shows that the majority of the population is at the low end of the lightning rates. Previous studies have shown similar cumulative distributions for oceanic lightning (Nesbitt et al. 2000; Petersen et al. 2005). The PDF for convective rainfall rate (Fig. 3) also shows an emphasis on the low end of the rainfall rates, although the slope of the curve is less steep than that of the lightning PDF.

Logarithmic and exponential distributions, such as those found in the analysis presented here, commonly occur in the atmosphere. The number density of the cumulus clouds has been observed to decrease nearly exponentially with increasing cloud size (e.g., Plank 1969). Drop size distribution is exponential (Marshall and Palmer 1948). Junge et al. (1969) and Bullrich et al. (1966) studied aerosol distribution in Pacific air masses and found sharp decay in the number of aerosol with aerosol radius. The distribution was approximated by a power law with an exponent between -3 and -4. Takahashi (1976), in a numerical study, found a logarithmic increase in rain rate when the number of cloud nuclei was decreased and approached a threshold value of 150 cm^{-3}. Foster et al. (2003) found an exponential growth of rain rate with precipitable water in Hawaii.

Physically, the logarithmic relationship between lightning and convective rainfall can be interpreted in the following way: assuming some CAPE and low-level moisture convergence over a limited area, a cloud starts to grow and the rainfall production is initiated relatively ''easily.'' The number of cloud condensation nuclei (CCN) has a great impact on the precipitation initiation and development (e.g., Takahashi 1976; Göke et al. 2007), but assuming relatively uniform aerosol content over the ocean, the available moisture content determines the maximum potential rainfall rate. Other environmental conditions have a weaker impact on the rainfall rate.

In contrast, the requirements for a robust charge-separation process are much more complex. Updraft speed, supercooled liquid water content, and ice content all need to be sufficient at the right altitude within a cloud. Other yet to be defined conditions may also play a role. Although weak cloud electrification is fairly common, the highest potential lightning rates are observed only on rare occasions when all the conditions for active lightning are met in a complex convective system.

It is suggested here that there are two fundamental factors that together determine the observed differences in lightning rates between the maritime and continental storms: (i) the number and distribution of CCN and ice nuclei (IN), and (ii) the vertical distribution of CAPE. The number of CCN–IN determines whether the cloud will develop having ''warm-cloud'' characteristics (maritime) with a small number of large droplets and rapid warm rain initiation or ''cold-cloud'' characteristics (continental) with the rainfall initiation triggered mainly by Wegener–Bergeron–Findeisen

process. On the other hand, the vertical distribution of instability (CAPE) has influence on the strength and height of the updraft. Together these two factors govern the ice and supercooled water mass flux in the mixed-phase region and determine the robustness of charge separation and cloud electrification. The confirmation of this hypothesis requires further studies using aerosol measurements together with lightning observations and soundings, followed by cloud model simulations that resolve the key elements.

These environmental circumstances and the results presented here suggest that the estimation of, for instance, rainfall rates from lightning rates is relatively insensitive at high lightning rates and more sensitive at low lightning rates. This is an encouraging result for lightning data assimilation applications, since the areas of strong storm activity and high rainfall rates, although less common, are the most important for NWP modeling.

Several studies have shown that lightning data can be assimilated into numerical models to help to improve the model forecasts (Alexander et al. 1999; Chang et al. 2001; Papadopoulos et al. 2005; Pessi et al. 2006). The lack of in situ data over the Pacific Ocean for initializing numerical models can lead to large forecast errors for storms that impact the west coast of North America or Hawaii. The results of this study suggest that the data from PacNet can be used as a proxy to estimate convective rainfall, latent heating, and hydrometeor profiles from lightning rates over the open ocean.

Acknowledgments. We are grateful to Ken Cummins and Nick Demetriades for their support in the development of PacNet and for providing PacNet data, to Joseph Nowak for help with detector site selection and installation, and to Nancy Hulbirt for assistance with graphics. TRMM 2A12 and 2A25 data products were obtained from the NASA Goddard Space Flight Center DAAC, and LIS data were obtained from the Global Hydrology Resource Center. This work is supported by the Office of Naval Research under Grants N00014-08-1-0450 and N00014-05-1-0551.

REFERENCES

Alexander, G. D., J. A. Weinman, V. M. Karyampudi, W. S. Olson, and A. C. L. Lee, 1999: The effect of assimilating rain rates derived from satellites and lightning on forecasts of the 1993 superstorm. *Mon. Wea. Rev.,* **127,** 1433–1457.

Anthes, R., Y.-H. Kuo, and J. R. Gyakum, 1983: Numerical simulations of a case of explosive marine cyclogenesis. *Mon. Wea. Rev.,* **111,** 1174–1188.

Blanchard, D. O., 1998: Assessing the vertical distribution of convective available potential energy. *Wea. Forecasting,* **13,** 870–877.

Boccippio, D. J., S. J. Goodman, and S. Heckman, 2000: Regional differences in tropical lightning distributions. *J. Appl. Meteor.,* **39,** 2231–2248.

——, K. L. Cummins, H. J. Christian, and S. J. Goodman, 2001: Combined satellite- and surface-based estimation of the intracloud–cloud-to-ground lightning ratio over the continental United States. *Mon. Wea. Rev.,* **129,** 108–122.

——, W. J. Koshak, and R. J. Blakeslee, 2002: Performance assessment of the Optical Transient Detector and Lightning Imaging Sensor. Part I: Predicted diurnal variability. *J. Atmos. Oceanic Technol.,* **19,** 1318–1332.

Brennan, M. J., and G. M. Lackmann, 2005: The influence of incipient latent heat release on the precipitation distribution of the 24–25 January 2000 U.S. East Coast cyclone. *Mon. Wea. Rev.,* **133,** 1913–1937.

Bullrich, K., R. Eiden, R. Jaenicke, and W. Nowak, 1966: Optical transmission of the atmosphere in Hawaii, II. Johannes Gutenberg University Final Tech. Rep., Contract DA-91-591-EUC-3458, 79 pp.

Businger, S., T. Birchard Jr., K. R. Kodama, P. A. Jendrowski, and J.-J. Wang, 1998: A bow echo and severe weather associated with a Kona low in Hawaii. *Wea. Forecasting,* **13,** 576–591.

Caruso, S. J., and S. Businger, 2006: Subtropical cyclogenesis over the central North Pacific. *Wea. Forecasting,* **21,** 193–205.

Cecil, D. J., S. J. Goodman, D. J. Boccippio, E. J. Zipser, and S. W. Nesbitt, 2005: Three years of TRMM precipitation features. Part I: Radar, radiometric, and lightning characteristics. *Mon. Wea. Rev.,* **133,** 543–566.

Chang, D.-E., J. A. Weinman, C. A. Morales, and W. S. Olson, 2001: The effect of spaceborne microwave and ground-based continuous lightning measurements on forecasts of the 1998 Groundhog Day storm. *Mon. Wea. Rev.,* **129,** 1809–1833.

Chèze, J.-L., and H. Sauvageot, 1997: Area-average rainfall and lightning activity. *J. Geophys. Res.,* **102,** 1707–1715.

Christian, H. J., Jr., 2006: Geostationary Lightning Mapper (GLM). Preprints, *12th Conf. on Aviation Range and Aerospace Meteorology*, Atlanta, GA, Amer. Meteor. Soc., J2.3.

——, R. J. Blakeslee, and S. J. Goodman, 1992: Lightning Imaging Sensor (LIS) for the Earth Observing System. NASA Tech. Memo. 4350, 36 pp.

——, and Coauthors, 2003: Global frequency and distribution of lightning as observed from space by the Optical Transient Detector. *J. Geophys. Res.,* **108,** 4005, doi:10.1029/2002JD002347.

Cram, R. S., and H. R. Tatum, 1979: Record torrential rains on the island of Hawaii, January–February 1979. *Mon. Wea. Rev.,* **107,** 1653–1662.

Del Genio, A. D., and W. Kovari, 2002: Climatic properties of precipitating convection under varying environmental conditions. *J. Climate,* **15,** 2597–2615.

DeMott, P. J., and D. C. Rogers, 1990: Freezing nucleation rates of dilute solution droplets measured between −30° and −40°C in laboratory simulations of natural clouds. *J. Atmos. Sci.,* **47,** 1056–1064.

Donaldson, R. J., 1961: Radar reflectivity profiles in thunderstorms. *J. Atmos. Sci.,* **18,** 292–305.

Ebert, E. E., and G. J. Holland, 1992: Observations of record cold cloud-top temperatures in Tropical Cyclone Hilda (1990). *Mon. Wea. Rev.,* **120,** 2240–2251.

Foote, G. B., and P. S. Du Toit, 1969: Terminal velocity of raindrops aloft. *J. Appl. Meteor.,* **8,** 249–253.

Foster, J., M. Bevis, Y.-L. Chen, S. Businger, and Y. Zhang, 2003: The Ka‘ū storm (November 2000): Imaging precipitable

water using GPS. *J. Geophys. Res.,* **108,** 4585, doi:10.1029/2003JD003413.

Futyan, J. M., and A. D. Del Genio, 2007a: Deep convective system evolution over Africa and the tropical Atlantic. *J. Climate,* **20,** 5041–5060.

——, and ——, 2007b: Relationships between lightning and properties of convective cloud clusters. *Geophys. Res. Lett.,* **34,** L15705, doi:10.1029/2007GL030227.

Göke, S., H. T. Ochs III, and R. M. Rauber, 2007: Radar analysis of precipitation initiation in maritime versus continental clouds near the Florida coast: Inferences concerning the role of CCN and giant nuclei. *J. Atmos. Sci.,* **64,** 3695–3707.

Grecu, M., and W. S. Olson, 2006: Bayesian estimation of precipitation from satellite passive microwave observations using combined radar–radiometer retrievals. *J. Appl. Meteor. Climatol.,* **45,** 416–433.

Iguchi, T., T. Kozu, R. Meneghini, J. Awaka, and K. Okamoto, 2000: Rain-profiling algorithm for the TRMM precipitation radar. *J. Appl. Meteor.,* **39,** 2038–2052.

Jorgensen, D. P., and M. A. LeMone, 1989: Vertically velocity characteristics of oceanic convection. *J. Atmos. Sci.,* **46,** 621–640.

Junge, C. E., E. Robinson, and F. L. Ludwig, 1969: A study of aerosols in Pacific air masses. *J. Appl. Meteor.,* **8,** 340–347.

Kelley, W. E., and D. R. Mock, 1982: A diagnostic study of upper tropospheric cold lows over the western North Pacific. *Mon. Wea. Rev.,* **110,** 471–480.

Kummerow, C., W. Barnes, T. Kozu, J. Shiue, and J. Simpson, 1998: The Tropical Rainfall Measuring Mission (TRMM) sensor package. *J. Atmos. Oceanic Technol.,* **15,** 809–817.

——, and Coauthors, 2001: The evolution of the Goddard profiling algorithm (GPROF) for rainfall estimation from passive microwave sensors. *J. Appl. Meteor.,* **40,** 1801–1820.

LeMone, M. A., and E. J. Zipser, 1980: Cumulonimbus vertical velocity events in GATE. Part I: Diameter, intensity and mass flux. *J. Atmos. Sci.,* **37,** 2444–2457.

Lucas, C., E. J. Zipser, and M. A. LeMone, 1994: Vertical velocity in oceanic convection off tropical Australia. *J. Atmos. Sci.,* **51,** 3183–3193.

Mackerras, D., M. Darveniza, R. E. Orville, E. R. Williams, and S. J. Goodman, 1998: Global lightning: Total, cloud and ground flash estimates. *J. Geophys. Res.,* **103,** 19 791–19 809.

Marshall, J. S., and W. M. Palmer, 1948: The distribution of raindrops with size. *J. Meteor.,* **5,** 165–166.

McCaul, E. W., Jr., and M. L. Weisman, 2001: The sensitivity of simulated supercell structure and intensity to variations in the shapes of environmental buoyancy and shear profiles. *Mon. Wea. Rev.,* **129,** 664–687.

McMurdie, L., and C. Mass, 2004: Major numerical forecast failures over the Northeast Pacific. *Wea. Forecasting,* **19,** 338–356.

Morrison, I., and S. Businger, 2001: Synoptic structure and evolution of a kona low. *Wea. Forecasting,* **16,** 81–98.

Nesbitt, S. W., E. J. Zipser, and D. J. Cecil, 2000: A census of precipitation features in the tropics using TRMM: Radar, ice scattering, and lightning observations. *J. Climate,* **13,** 4087–4106.

Olson, W. S., and Coauthors, 2006: Precipitation and latent heating distributions from satellite passive microwave radiometry. Part I: Improved method and uncertainties. *J. Appl. Meteor. Climatol.,* **45,** 702–720.

Otkin, J. A., and J. E. Martin, 2004: A synoptic climatology of the subtropical kona storm. *Mon. Wea. Rev.,* **132,** 1502–1517.

Papadopoulos, A., T. G. Chronis, and E. N. Anagnostou, 2005: Improving convective precipitation forecasting through assimilation of regional lightning measurements in a mesoscale model. *Mon. Wea. Rev.,* **133,** 1961–1977.

Pessi, A., S. Businger, and T. Cherubini, 2006: Comparison of two methods for assimilation of lightning data into NWP models. Preprints, *First Int. Lightning Meteorology Conf.*, Tucson, AZ, Vaisala, CD-ROM.

——, ——, K. L. Cummins, N. W. S. Demetriades, M. Murphy, and B. Pifer, 2009: Development of a long-range lightning detection network for the Pacific: Construction, calibration, and performance. *J. Atmos. Oceanic Technol.,* **26,** 145–166.

Petersen, W. A., and S. A. Rutledge, 1998: On the relationship between cloud-to-ground lightning and convective rainfall. *J. Geophys. Res.,* **103,** 14 025–14 040.

——, ——, and R. E. Orville, 1996: Cloud-to-ground lightning observations from TOGA COARE: Selected results and lightning location algorithms. *Mon. Wea. Rev.,* **124,** 602–620.

——, ——, R. C. Cifelli, B. S. Ferrier, and B. F. Smull, 1999: Shipborne dual-Doppler operations during TOGA COARE: Integrated observations of storm kinematics and electrification. *Bull. Amer. Meteor. Soc.,* **80,** 81–97.

——, H. J. Christian, and S. A. Rutledge, 2005: TRMM observations of the global relationship between ice water content and lightning. *Geophys. Res. Lett.,* **32,** L14819, doi:10.1029/2005GL023236.

Phillips, V. T. J., L. J. Donner, and S. T. Garner, 2007: Nucleation processes in deep convection simulated by a cloud-system-resolving model with double-moment bulk microphysics. *J. Atmos. Sci.,* **64,** 738–761.

Pierce, E., 1970: Latitudinal variation of lightning parameters. *J. Appl. Meteor.,* **9,** 194–195.

Plank, V. G., 1969: The size distribution of cumulus clouds in representative Florida populations. *J. Appl. Meteor.,* **8,** 46–67.

Prentice, S. A., and D. Mackerras, 1977: The ratio of cloud to cloud-ground lightning flashes in thunderstorms. *J. Appl. Meteor.,* **16,** 545–549.

Price, C., and D. Rind, 1993: What determines the cloud-to-ground lightning fraction in thunderstorms? *Geophys. Res. Lett.,* **20,** 463–466.

Pruppacher, H. R., and J. D. Klett, 1978: *Microphysics of Clouds and Precipitation*. D. Reidel, 714 pp.

Rutledge, S. A., E. R. Williams, and T. D. Keenan, 1992: The Down Under Doppler and Electricity Experiment (DUNDEE): Overview and preliminary results. *Bull. Amer. Meteor. Soc.,* **73,** 3–16.

Sadler, J. C., and Coauthors, 1975: The upper tropospheric circulation over the global tropics. Department of Meteorology, University of Hawaii Tech. Rep. UHMET-75-05. [Available online at http://www.soest.hawaii.edu/Library/Sadler.html.]

Saunders, C., 1993: A review of thunderstorm electrification processes. *J. Appl. Meteor.,* **32,** 642–655.

Sherwood, S. C., V. T. J. Phillips, and J. S. Wettlaufer, 2006: Small ice crystals and the climatology of lightning. *Geophys. Res. Lett.,* **33,** L05804, doi:10.1029/2005GL025242.

Soriano, L. R., F. de Pablo, and E. G. Díez, 2001: Relationship between convective precipitation and cloud-to-ground lightning in the Iberian Peninsula. *Mon. Wea. Rev.,* **129,** 2998–3003.

Szoke, E. J., E. J. Zipser, and D. P. Jorgensen, 1986: A radar study of convective cells in mesoscale systems in GATE. Part I: Vertical profile statistics and comparison with hurricanes. *J. Atmos. Sci.,* **43,** 182–198.

Takahashi, T., 1976: Warm rain, giant nuclei and chemical balance—A numerical model. *J. Atmos. Sci.,* **33,** 269–286.

——, 1978: Electrical properties of oceanic tropical clouds at Ponape, Micronesia. *Mon. Wea. Rev.,* **106,** 1598–1612.

——, 1984: Thunderstorm electrification—A numerical study. *J. Atmos. Sci.,* **41,** 2541–2558.

——, 1990: Near absence of lightning in torrential rainfall producing Micronesian thunderstorms. *Geophys. Res. Lett.,* **17,** 2381–2384.

Tapia, A., J. A. Smith, and M. Dixon, 1998: Estimation of convective rainfall from lightning observations. *J. Appl. Meteor.,* **37,** 1497–1509.

Toracinta, E. R., K. I. Mohr, E. J. Zipser, and R. E. Orville, 1996: A comparison of WSR-88D reflectivities, SSM/I brightness temperatures, and lightning for mesoscale convective systems in Texas. Part I: Radar reflectivity and lightning. *J. Appl. Meteor.,* **35,** 902–918.

——, D. J. Cecil, E. J. Zipser, and S. W. Nesbitt, 2002: Radar, passive microwave, and lightning characteristics of precipitating systems in the tropics. *Mon. Wea. Rev.,* **130,** 802–824.

Wang, C. P., 1963: Lightning discharges in the tropics, 1. Whole discharges. *J. Geophys. Res.,* **68,** 1943–1949.

Williams, E. R., 1985: Large-scale charge separation in thunderclouds. *J. Geophys. Res.,* **90** (D4), 6013–6025.

——, K. Rothkin, D. Stevenson, and D. Boccippio, 2000: Global lightning variations caused by changes in thunderstorm flash rate and by changes in the number of thunderstorms. *J. Appl. Meteor.,* **39,** 2223–2230.

Yang, S., W. S. Olson, J. J. Wang, T. L. Bell, E. A. Smith, and C. D. Kummerow, 2006: Precipitation and latent heating distributions from satellite passive microwave radiometry. Part II: Evaluation of estimates using independent data. *J. Appl. Meteor. Climatol.,* **45,** 721–739.

Zipser, E. J., 1970: The Line Island Experiment: Its place in tropical meteorology and the rise of the fourth school of thought. *Bull. Amer. Meteor. Soc.,* **51,** 1136–1146.

——, 1994: Deep cumulonimbus cloud systems in the tropics with and without lightning. *Mon. Wea. Rev.,* **122,** 1837–1851.

——, and M. LeMone, 1980: Cumulonimbus vertical velocity events in GATE. Part II: Synthesis and model core structure. *J. Atmos. Sci.,* **37,** 2458–2469.

——, and K. R. Lutz, 1994: The vertical profile of radar reflectivity of convective cells: A strong indicator of storm intensity and lightning probability? *Mon. Wea. Rev.,* **122,** 1751–1759.